European Journal of Oral Sciences

Eur J Oral Sci 2011; 119 (Suppl. 1): 168–176
DOI: 10.1111/j.1600-0722.2011.00904.x
Printed in Singapore. All rights reserved

European Journal of Oral Sciences

Epithelial-specific knockout of the *Rac1* gene leads to enamel defects

Zhan Huang[1], Jieun Kim[2], Rodrigo S. Lacruz[1], Pablo Bringas Jr[1], Michael Glogauer[3], Timothy G. Bromage[4], Vesa M. Kaartinen[2], Malcolm L. Snead[1]

[1]The Center for Craniofacial Molecular Biology, Herman Ostrow School of Dentistry, University of Southern California, Los Angeles, CA, USA; [2]Department of Biologic and Materials Sciences, School of Dentistry, University of Michigan, Ann Arbor, MI, USA; [3]Matrix Dynamics Group, Faculty of Dentistry, University of Toronto, Toronto, Ontario, Canada; [4]New York University College of Dentistry, New York, NY, USA

Huang Z, Kim J, Lacruz RS, Bringas P Jr, Glogauer M, Bromage TG, Kaartinen VM, Snead ML. Epithelial-specific knockout of the Rac1 *gene leads to enamel defects. Eur J Oral Sci 2011; 119 (Suppl. 1): 168–176. © 2011 Eur J Oral Sci*

The Ras-related C3 botulinum toxin substrate 1 (*Rac1*) gene encodes a 21-kDa GTP-binding protein belonging to the RAS superfamily. RAS members play important roles in controlling focal adhesion complex formation and cytoskeleton contraction, activities with consequences for cell growth, adhesion, migration, and differentiation. To examine the role(s) played by RAC1 protein in cell–matrix interactions and enamel matrix biomineralization, we used the *Cre*/*loxP* binary recombination system to characterize the expression of enamel matrix proteins and enamel formation in *Rac1* knockout mice ($Rac1^{-/-}$). Mating between mice bearing the floxed *Rac1* allele and mice bearing a cytokeratin 14-*Cre* transgene generated mice in which *Rac1* was absent from epithelial organs. Enamel of the *Rac1* conditional knockout mouse was characterized by light microscopy, backscattered electron imaging in the scanning electron microscope, microcomputed tomography, and histochemistry. Enamel matrix protein expression was analyzed by western blotting. Major findings showed that the Tomes' processes of $Rac1^{-/-}$ ameloblasts lose contact with the forming enamel matrix in unerupted teeth, the amounts of amelogenin and ameloblastin are reduced in $Rac1^{-/-}$ ameloblasts, and after eruption, the enamel from $Rac1^{-/-}$ mice displays severe structural defects with a complete loss of enamel. These results support an essential role for RAC1 in the dental epithelium involving cell–matrix interactions and matrix biomineralization.

Zhan Huang, The Center for Craniofacial Molecular Biology, The Herman Ostrow School of Dentistry, University of Southern California, HSC, CSA 142 2250 Alcazar Street, Los Angeles, CA 90033, USA

Telefax: +1–323–4422981
E-mail: zhanhuan@usc.edu

Key words: ameloblast; cell adhesion; epithelial cell; extracellular matrix; *Rac1*

Accepted for publication September 2011

Enamel, the hardest and most mineralized tissue in the vertebrate body, is formed by ameloblasts through the coordinated processes of morphogenesis and cytodifferentiation, which are signaled by sequential and reciprocal epithelial–mesenchymal interactions (1–3).

Ras-related C3 botulinum toxin substrate 1 (RAC1), a 21-kDa small GTP-binding protein, belongs to the RAS superfamily whose members play important roles in controlling cell growth, migration, and differentiation. RAC1 proteins are required for assembly of the actin cytoskeleton and their associated focal complexes, and are essential for the formation of three germ layers during early mouse embryogenesis (4, 5).

Deletion of *Rac1* in murine neural crest cells results in abnormal craniofacial development with clefting at embryonic day 12 (E12), evidenced by disrupted integrity of the craniofacial and pharyngeal mesenchyme. Animals with the binary deletion (*Rac1*/*Wnt1-Cre*) die at an early embryonic stage (6). *Rac1*-null mouse embryonic fibroblasts are contracted in morphology and defective in lamellipodia formation, cell spreading, cell–fibronectin adhesion, and focal contact formation in response to platelet-derived growth factor or serum (7). Animals with the binary deletion (*Rac1*/cytokeratin 14) exhibit a clearly delayed closure and healing of cutaneous and oral wounds (8). Whether RAC1 is required for enamel development is not fully understood. To investigate the role played by RAC1 in cell–matrix interactions and in subsequent matrix biomineralization during enamel formation, we used the *Cre*/*loxP* recombination system to characterize enamel matrix protein expression in *Rac1* conditional knockout mice in which the cytokeratin 14 (keratin 14) promoter drives *Cre* expression in epithelial organs.

Integrin cell receptors on the ameloblast surface have been shown to participate in amelogenesis by mediating cell adhesion with the enamel extracellular matrix proteins through several ligands and specific signals that result from these interactions (9–11). Integrin $\alpha6\beta4$ interacts with the laminin $\alpha5$ chain and regulates the cell polarity of inner dental epithelium via the RAC/CDC42 pathway, thus participating in determining the start of ameloblast differentiation (12). On the other hand, attachment of cells to the extracellular matrix results in the clustering of integrins and the formation of focal complexes, which are associated with a variety of dynamic changes in cytoplasmic proteins and the organization of the actin cytoskeleton for maintaining cell growth, survival, and directing cell migration (13). It has been suggested that the cytoskeletal organization in ameloblasts may determine the formation of distal terminal junction complexes and the cyclic activity of ameloblast secretory end-pieces known as Tomes' processes and be involved in pattern formation of the enamel matrix (14–17).

Material and methods

Mouse preparation

The Keratin 14 promoter (*K14*)-*Cre* transgenic line, and the $Rac1^{fl/fl}$ (fl, flanked by loxP sites) mouse stain have been described previously (4, 6, 18). Mating *K14-Cre*$^{+/-}$ with fl/fl ($Rac1^{fl/fl}$) mice generated wild-type/fl and *K14-Cre* mice. Subsequent mating between wild-type/fl; *K14-Cre* mice generated fl/fl and *K14-Cre* homozygous conditional *Rac1* knockout mice. For ease of identification, we refer to the wild-type animal as $Rac1^{+/+}$ (WT), the wild-type/fl; *K14-Cre* animal as $Rac1^{+/-}$, and the fl/fl; *K14-Cre* animal as $Rac1^{-/-}$. The Institutional Animal Care and Use Committee (IACUC) approved this study. Animals at selected stages of development were examined, and this study focused on newborn, postnatal day-2 (PN2), postnatal day-12 (PN12), and postnatal day-61 (PN61) mice.

Genotyping of *Rac1* alleles

Genomic DNA was isolated by digestion in a buffer containing 0.6 mg ml^{-1} of proteinase K, 50 mM Tris–HCl, pH 8.0, 100 mM EDTA, and 0.5% SDS (Sigma, St Louis, MO, USA) at 55°C overnight. The solution was subjected to extraction with phenol, phenol/chloroform, and chloroform. DNA in the aqueous phase was precipitated by the addition of two volumes of ethanol. An additional wash step in 70% ethanol was essential to remove traces of SDS and phenol before biochemical manipulation. The PCR primers PO33 (TCCAATCTGTGCTGCCCATC), PO45 (CAGAGCTCGAATCCAGAAACTAGTA), and PO91 (GATGCTTCTAGGGGTGAGCC) were used in multiplex PCR reactions to differentiate the various wild-type, floxed *Rac1*, or knockout *Rac1* alleles. The PO33/PO45 primer pair was used to detect the 115-bp wild-type allele, the PO33/PO91 primer pair was used to detect the 242-bp floxed *Rac1* allele, and the PO45/PO91 primer pair was used to detect the 140-bp knockout allele. The primer pair used to identify the 700-bp *Cre* allele was: forward primer, 5′-TGCTGTTTCACTGGTTATGCGG-3′, and reverse primer, 5′-CCATTGCCCCTGTTTCACTATCC-3′.

Backscattered electron imaging in the scanning electron microscope

Hemimandibles of PN12 and PN61 wild-type or $Rac1^{-/-}$ mice were dissected, fixed in 4% paraformaldehyde overnight, dehydrated in graded concentrations of acetone, and embedded in epoxy resin. Embedded blocks were sectioned in the coronal plane between the first and second molars, effectively sampling the mandibular incisor deep within the jaw at the same relative location for all specimens. One surface of each block was polished, made electrically conductive with a carbon coating, and examined in a Zeiss EVO-50 scanning electron microscope by backscattered electron imaging at high vacuum with an accelerating voltage of 50 kV, 50 pA specimen current, and a 9 mm working distance.

Microcomputed tomography

Mandibles from wild-type or $Rac1^{-/-}$ PN12 or PN61 mice were dissected, fixed, and preserved in 70% alcohol. The samples were analyzed using the MicroCAT II (Siemens Medical Solutions, Knoxville, TN, USA). The microcomputed tomography images were acquired with an X-ray source operating at 80 kV and 250 μA. The data were collected at 10 μm resolution per voxel.

Western blotting

Protein recovery, resolution to size, and detection by a specific antibody was performed as previously described (19). Mandibular first molars from PN2 wild-type or $Rac1^{-/-}$ mice were dissected and washed in ice-cold PBS, and then in 100 μl of ice-cold RIPA buffer (1 × PBS, 1% Nonidet P-40, 0.1 mg ml^{-1} of phenylmethanesulfonyl fluoride, 30 μl ml^{-1} of aprotinin, and 1 mM sodium orthovanadate) (Sigma). The lysate was cleared by centrifugation at 21,800 *g* for 15 min at 4°C, and the protein concentration of the supernatant was measured using a Bio-Rad protein assay kit (Bio-Rad, Hercules, CA, USA) with serial dilutions of BSA as a standard. Experimental samples were electrophoretically resolved to size on a 4–12% SDS-polyacrylamide gradient gel (Invitrogen, Carlsbad, CA, USA) and transferred to Immobilon-P membrane (Millipore, Temecula, CA, USA). The membranes were incubated in blocking buffer overnight at 4°C, then incubated with primary antibody (chicken anti-recombinant mouse amelogenin polyclonal IgY (1:3,000 dilution) (20) or rabbit anti-recombinant rat ameloblastin polyclonal IgG (1:2,000 dilution) as previously described (21)] for 1 h and detected by incubation with a secondary antibody (horseradish peroxidase-conjugated anti-chicken or anti-rabbit IgG) for 1 h at room temperature. Proteins were visualized by enhanced chemiluminescence (GE Healthcare, Pittsburgh, PA, USA).

Immunohistochemistry

Immunostaining was performed as described previously (22). Briefly, hemimandibles from newborn or PN2 wild-type and $Rac1^{-/-}$ mice were dissected and fixed overnight in freshly prepared 4% paraformaldehyde in PBS, pH 7.4, at 4°C. Tissue sections of 6 μm thickness were prepared and blocked to prevent non-specific absorption. After incubation with the selected primary antibody, the localization of the antibody–antigen complex was visualized with a suitable chromogen. Polyclonal anti-mouse amelogenin IgY (1:1,000 dilution) was raised in chicken and recovered from the egg yolk, an anti-chicken horseradish peroxidase-conjugated secondary antibody IgG (1:1,500 dilution), (Invitrogen), and a peroxidase substrate (AEC) was used for detection by local precipitation of the visible chromogen.

Unless stated otherwise all chemicals and reagents were from Sigma.

Results

General phenotypes of *Rac1* conditional knockout mice

Approximately 60% of *Rac1*-deficient mice were born dead, and pups alive at birth were indistinguishable from wild-type mice. However, within the first week of birth it became obvious that mice with the *Rac1* deletion had a smaller body size, grew less hair, and displayed progressive hair loss, as reported previously (23). At PN12, the gross appearance of wild-type and $Rac1^{+/-}$ animals was similar, while $Rac1^{-/-}$ lost almost all of their body hair (Fig. 1A). Genotyping results are shown in Fig. 1

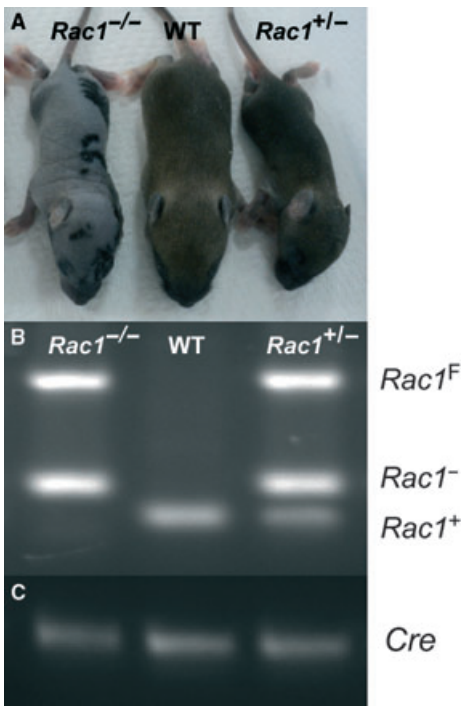

Fig. 1. Gross appearance and genotyping results of wild-type (WT) and $Rac1^{-/-}$ mice. (A) Gross appearance of postnatal day-12 (PN12) $Rac1^{-/-}$, WT, and $Rac1^{+/-}$ animals. (B, C) Genotyping results of loxP-targeted (F), wild-type (+), and *Cre*-mediated recombination (−) for *Rac1* alleles. The product sizes of the amplified alleles were: 242 bp for the $Rac1^{F}$ floxed allele, 140 bp for the $Rac1^{-}$ knockout allele, 115 bp for the $Rac1^{+}$ wild-type allele, and 700 bp for the *Cre* allele.

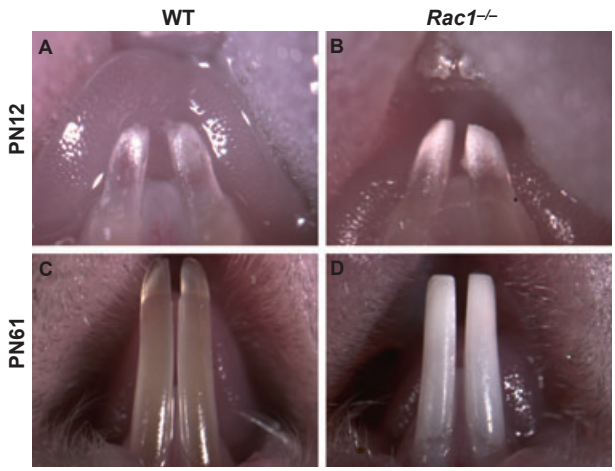

Fig. 2. Physical appearance of wild-type and $Rac1^{-/-}$ mouse mandibular teeth. Mandibular incisors of wild-type (WT) postnatal day-12 (PN12) (A) and postnatal day-61 (PN61) (C) mice are compared with those of $Rac1^{-/-}$ PN12 (B) and PN61 (D) littermates, respectively. The appearance of the dental enamel in $Rac1^{-/-}$ incisors was abnormal, with a white chalky color. The enamel layer on the surface of incisors was almost entirely lost in PN61 *Rac1* null mice (D).

B,C. The size of the amplified product for the $Rac1^{F}$ floxed allele was 242 bp, that of the $Rac1^{+}$ wild-type allele was 115 bp, and that of the $Rac1^{-}$ null allele was 140 bp, as shown in Fig. 1B. The internal control of the *Cre* gene is shown in Fig. 1C. $Rac1^{-/-}$ mice had a shorter life expectancy compared with their wild-type siblings, and died at around 2–6 months of age from digestive tract defects (24).

Dental defects in *Rac1* conditional knockout mice

$Rac1^{-/-}$ mice were fully dentate, as observed grossly or in histological sectioning, or by image analysis. The appearance of PN12 mandibular incisors from wild-type (Fig. 2A) and $Rac1^{-/-}$ (Fig. 2B) mice or of PN61 mandibular incisors from wild-type (Fig. 2C) and $Rac1^{-/-}$ (Fig. 2D) mice is shown. Dental enamel in $Rac1^{-/-}$ mouse molars and incisors was abnormal, with a white or chalky appearance that lacked the iron pigment normally seen in wild-type mouse teeth. After tooth eruption, the enamel on the surfaces of incisors (Fig. 2) and molars (data not shown) was lost to abrasion or attrition through mastication.

Backscattered electron images, viewed by scanning electron microscopy, of the sectioned mandibular incisors from wild-type and $Rac1^{-/-}$ mice are shown in Fig. 3. Enamel from $Rac1^{-/-}$ mandibular incisors at PN12 (Fig. 3B,D) or PN61 (Fig. 3F,H) generated a reduced backscattered electron signal compared with enamel from wild-type littermates at PN12 (Fig. 3A,C) or PN61 (Fig. 3E,G), indicating that the enamel in the *Rac1*-deleted mice is hypomineralized compared with wild-type controls. In addition, enamel from the *Rac1*-deleted mouse revealed modest disruption of the enamel rod architecture (Fig. 3D). Part of the enamel surface in PN12 $Rac1^{-/-}$ mouse incisor appeared collapsed, as shown in Fig. 3B,D.

Micro-computed tomography images showed the presence of mandibular incisors and molars from PN12 and PN61 wild-type and $Rac1^{-/-}$ littermates, respectively (Fig. 4). For both developmental periods, the images demonstrated a lower density of the enamel layer in the $Rac1^{-/-}$ mice (Fig. 4B,D) compared with that of wild-type mice (Fig. 4A,C). Notably, at PN61 the majority of the enamel layer from the incisor of the $Rac1^{-/-}$ mice was lost from the incisal edge to the mid-length of the erupted incisor (Fig. 4D).

Morphological characteristics of enamel-secreting ameloblasts

Mouse mandibular incisors were chosen for this study because they display a gradient of ameloblast differentiation along their rostral-caudal longitudinal axis, with a stem cell population at their growing end that continues through to fully mature enamel at the most incisal end. Surprisingly, the microanatomy of the incisor tooth organ, including the ameloblasts, at the presecretory phase, reveals very few gross disturbances for the $Rac1^{-/-}$ (Fig. 5H) vs. wild-type (Fig. 5G) incisor teeth at PN2. It is not until the later stages of secretion that the major findings from the hematoxylin and eosin staining of these samples are revealed. Here, we found that the apical

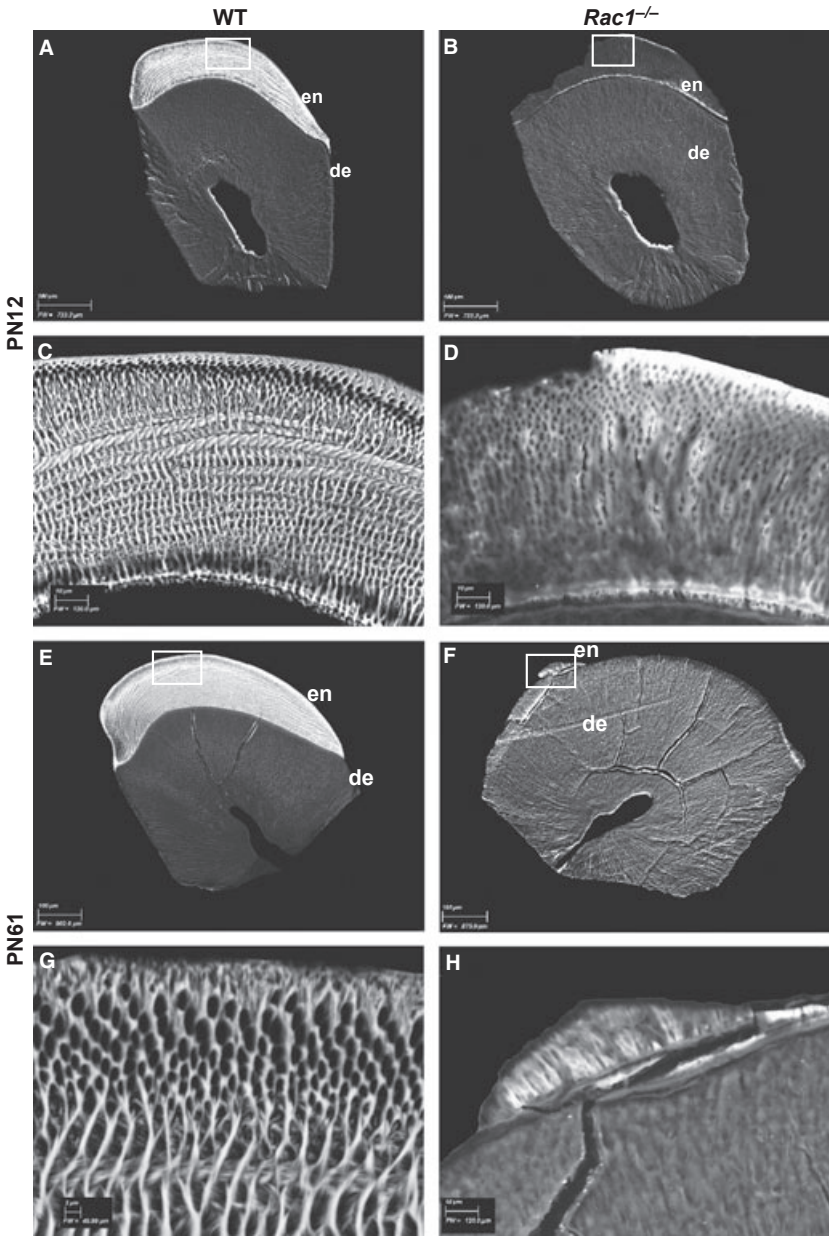

Fig. 3. Backscattered scanning electron microscopy images of mandibular incisors from wild-type (WT) and *Rac1*$^{-/-}$ mice are shown in cross-section. Mandibular enamel from postnatal day-12 (PN12) *Rac1*$^{-/-}$ (B, D) and postnatal day-61 (PN61) (F, H) mouse incisors generated a reduced backscattered electron signal compared with enamel from mandibular incisors of WT PN12 (A, C) and PN61 (E, G) littermates, respectively. de, dentin; en, enamel.

surface of enamel-secreting ameloblasts, known as Tomes' processes, at both early-secretory (Fig. 5F,L) and late-secretory (Fig. 5D,J) stages, became shortened and disoriented in *Rac1*-deleted animals compared with wild-type secretory ameloblasts (Fig. 5E,K vs. Fig. 5C,I) at these same developmental stages, respectively. Although ameloblast cell polarity and columnar shape does not appear to be altered, the normal cell–cell and cell–enamel matrix contacts are lost in the unerupted mandibular incisor from the *Rac1*$^{-/-}$ mouse along the entirety of the developmental gradient of palisading ameloblasts (Fig. 5D,F,H), compared with similar features from *Rac1* wild-type mouse incisors (Fig. 5C,E,G).

Enamel matrix proteins in *Rac1* conditional knockout mice

The expression of the two most abundant enamel matrix proteins secreted by ameloblast cells – amelogenin and ameloblastin – were examined by western blotting in mouse molars recovered from PN2 animals (Fig. 6). We found that the abundance of the major enamel matrix proteins, amelogenin (Fig. 6A) and ameloblastin (Fig. 6 B) were remarkably reduced.

We also examined amelogenin protein expression using immunohistochemistry techniques to determine if changes in expression levels had occurred in ameloblasts

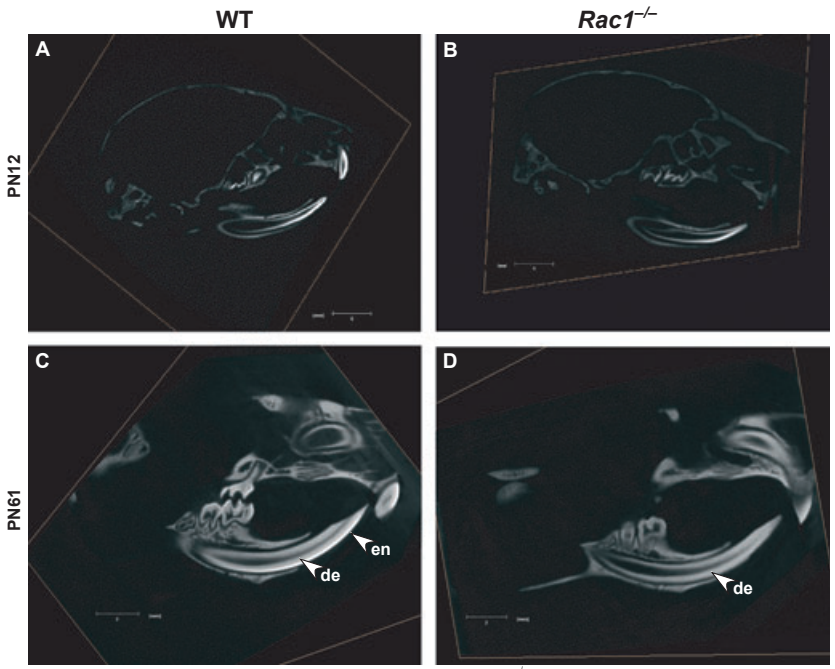

Fig. 4. Computed tomography of the heads from wild-type (WT) and *Rac1*$^{-/-}$ mice. Mandibular incisors from WT postnatal day-12 (PN12) (A) and postnatal day-61 (PN61) (C) mice were compared with those from *Rac1*$^{-/-}$ PN12 (B) and PN61 (D) littermates. PN61 *Rac1*$^{-/-}$ mandibular molars and incisors (D) demonstrated abnormal, flat, and worn enamel. The enamel layer from the incisal edge to the mid-length of the erupted incisor in PN61 *Rac1*$^{-/-}$ mice was lost (D). de, dentin; en, enamel.

globally or regionally with the elimination of the *Rac1* gene. To accomplish this, we examined newborn incisors at a developmental site where amelogenin is initially secreted by newly differentiated ameloblasts (Fig. 7A,B). Immunostaining showed that while amelogenin was detectable, its abundance in newborn *Rac1*$^{-/-}$ mouse mandibular incisor (Fig. 7D,F) was reduced compared with the corresponding features in wild-type ameloblasts (Fig. 7C,E).

Discussion

Tooth enamel formation, also known as amelogenesis, is coordinated with the formation of dentin by odontoblasts when the inner enamel epithelial cells proliferate and form the contours of the dentino–enamel junction. The inner enamel epithelial cells continue their exchange of signals with dentinoblasts, resulting in the elongation, polarization, and differentiation of pre-ameloblasts, which differentiate into secretory ameloblasts and form an enamel matrix. Initially, the ameloblasts make contact with the proteins within the basement membrane that separates the inner enamel epithelial cells from the presumptive dentinoblasts. With the synthesis and secretion of the enamel extracellular matrix, the Tomes' processes of the secretory ameloblasts remain in contact with the mineralizing enamel ceramic composite. Disturbances in either the process of ameloblast differentiation, or in the secretion or maturation of the enamel matrix can lead to defects in the enamel bioceramic (20, 25, 26). Mutations in human genes such as amelogenin, X-linked (*AMELX*), enamelin (*ENAM*), kallikrein-related peptidase 4 (*KLK4*), and matrix metalloproteinase 20 (*MMP20*) form the molecular basis for a series of defects in enamel formation known as amelogenesis imperfecta (AI). In AI, a defective protein structure encoded by the mutated gene can result in specific defects in enamel formation (27–30). Enamel from AI sources or teeth with enamel hypoplasia or hypomaturation accumulate mechanical defects that result in weak and easily damaged enamel.

The *Rho* family of small guanine nucleotide (GTP)-binding proteins consists of RHO, RAC, and CDC42 subfamilies, among which RHOA, RAC1, and CDC42 are expressed and differently distributed at selected stages of tooth development and may play essential roles during amelogenesis. Recent studies showed that the abolishment of amelogenin mRNA expression and the loss of regular palisade-like organization of ameloblasts present in tooth germs cultured with *Clostridium difficile* toxin A inhibited all Rho-GTPase activity, while specific inhibition of *Rock*, an effector of the *RhoA* pathway, partially reduced the expression of amelogenin but predominately affected odontoblasts (31). The expression of a dominant negative *RhoA* in ameloblasts led to enamel hypoplasia with surface defects (32). However, the role(s) and function(s) of RAC1 during the formation and development of enamel have not been further elucidated. Experimentally, this can be accomplished by a gain-of-function approach, as in transgenic animals, or through loss of function in null animals. To avoid embryonic lethality, we used a loss of function approach restricted to a specific germ layer compartment by using a binary ablation technique. *K14-Cre* transgene-mediated DNA recombination occurs uniformly and consistently in enamel organ epithelia, as previously reported (19).

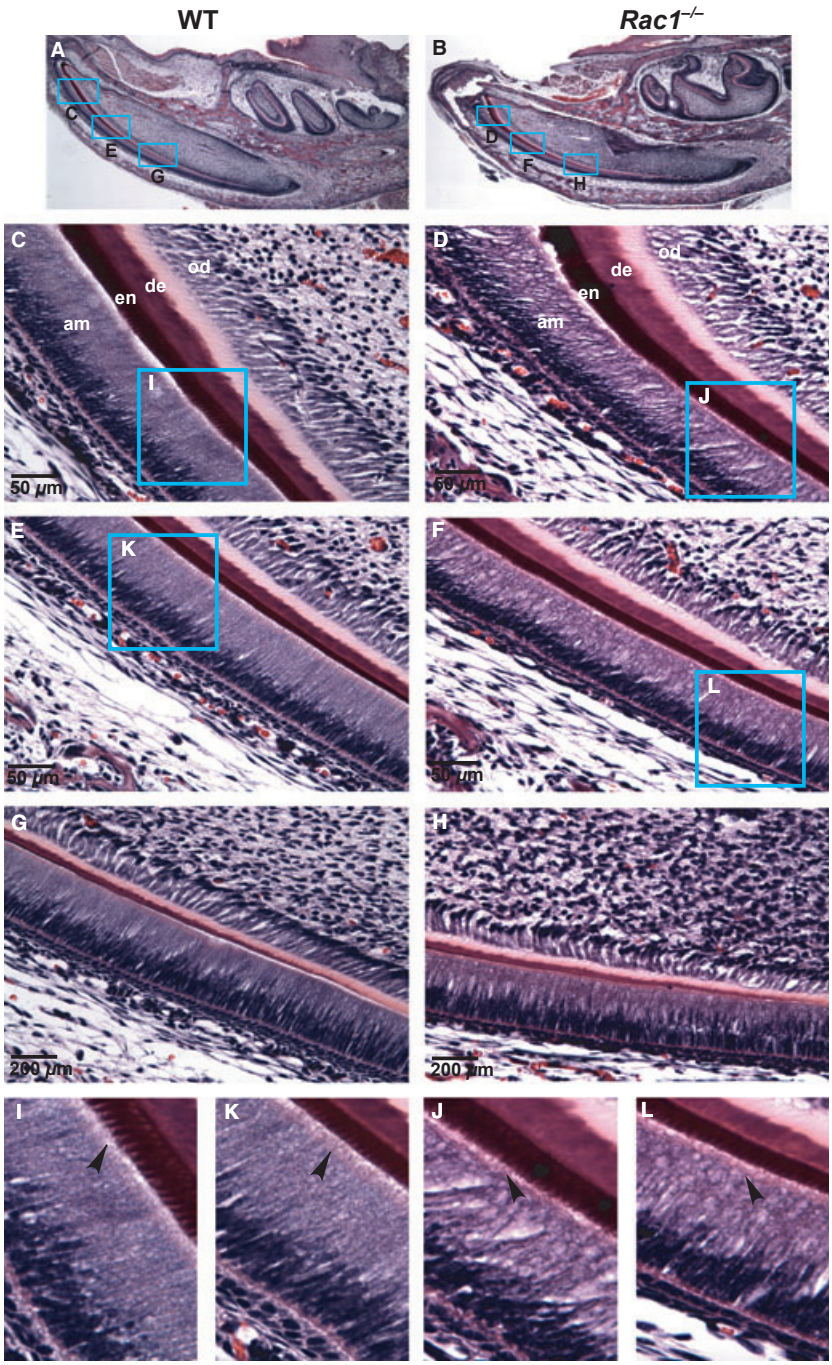

Fig. 5. Morphological characteristics of enamel-secreting ameloblasts from mandibular incisors of postnatal day-2 (PN2) wild-type (WT) and *Rac1*$^{-/-}$ mice. Specific regions along the rostral-to-caudal developmental gradient of dental epithelia were chosen in order to study the cell microanatomy indicative of morphological differentiation in late secretory (C, D), early secretory (E, F), and late presecretory stage (G, H) ameloblasts in PN2 WT (A) and the *Rac1*$^{-/-}$ mouse (B) mandibular incisor using standard hematoxylin and eosin staining. The Tomes' processes, specialized regions found at the apical end of ameloblasts, in early- (L), and late- (J) secretory stages of development, were shortened and lost contact with the forming enamel matrix in PN2 *Rac1*$^{-/-}$ mouse when compared with early- (K) and late- (I) secretory ameloblasts in wild-type animal. am, ameloblast; de, dentin; en, enamel; od, odontoblasts.

In PN2 mouse molars from the *Cre*-mediated deletion of *Rac1*, expression of both amelogenin and ameloblastin was significantly reduced; at PN12 and PN61, *Rac1* conditional knockout mice exhibited disturbances to enamel formation, including the presence of hypoplasia and subsurface hypomineralization at various depths and to different extents, resulting in a phenotype similar to some forms of AI in humans. The dominant protein of mammalian enamel is amelogenin, while the second most abundant enamel structural protein of the forming enamel matrix is ameloblastin, also known as sheathelin (20, 33). Amelogenin and ameloblastin double-knockout

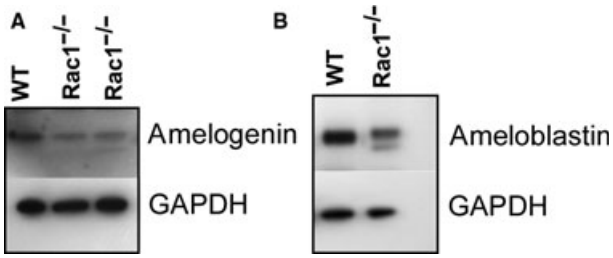

Fig. 6. Expression of enamel matrix proteins in postnatal day-2 (PN2) wild-type (WT) and *Rac1*$^{-/-}$ mice. The expression of the dominant and second most abundant enamel matrix proteins secreted by ameloblast cells, amelogenin (A) and ameloblastin (B), were examined by western blotting of mouse molars extracted from WT or *Rac1*$^{-/-}$ PN2 animals. GAPDH, glyceraldehyde-3-phosphate dehydrogenase.

mice showed additional enamel defects in comparison with amelogenin or ameloblastin single null mice, suggesting the synergistic roles of the dominant matrix proteins during enamel formation and mineralization (34–36). Previous investigators have suggested that amelogenins are required for the organization and orientation of hydroxyapatite crystallites during enamel development, while ameloblastin is essential for maintaining ameloblast cyto-differentiation and cell attachment (26, 33, 35, 37, 38). The decreased expression of amelogenin and ameloblastin in RAC1 conditional deleted mouse incisors supports a central role for *Rac1* in acquiring and maintaining the state of ameloblast differentiation. Disruption between the integrins and other potential enamel matrix protein receptors are operationalized by the absence of the RAC1 protein in the null animals. The absence of RAC1 may also be responsible for the altered cell–matrix interaction observed in the Tomes' processes of the *Rac1*$^{-/-}$ animals in this study.

Rho-GTPases mediate a variety of essential biological functions by triggering signaling pathways related to cell morphology and motility. The RHOA pathway is involved in cell cycle or gene transcription regulation during ameloblast differentiation (39). The RAC1 signaling pathway is known to regulate the formation of

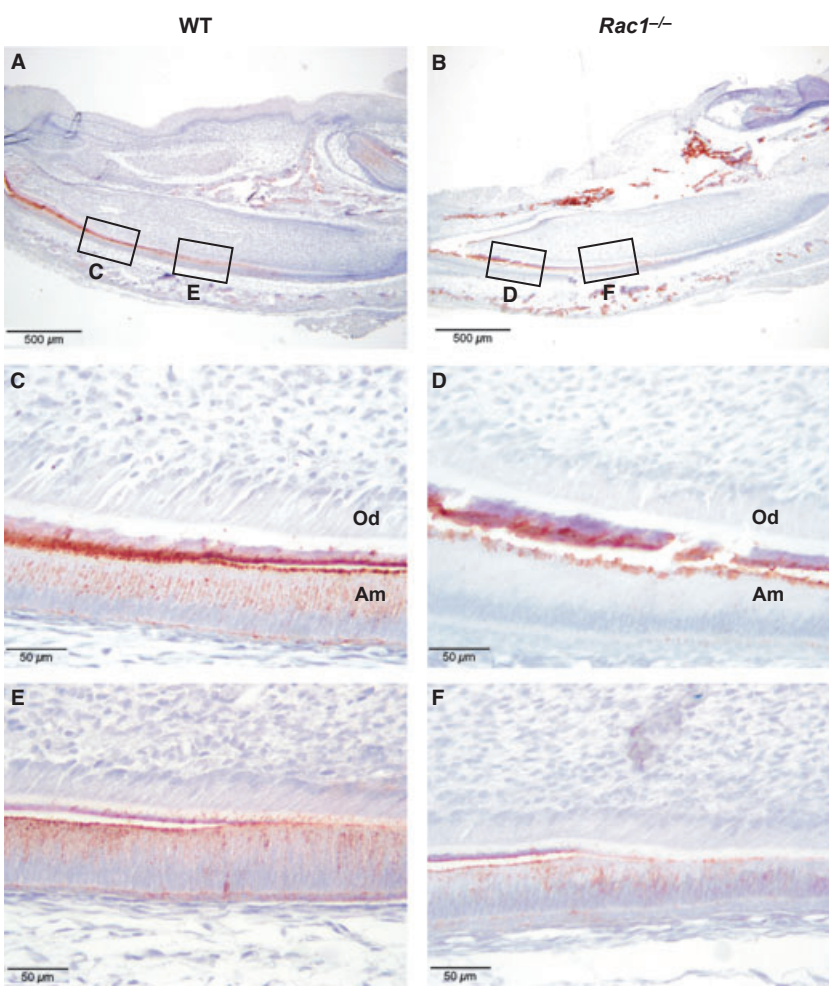

Fig. 7. Immunostaining of amelogenin in the sagittal sectioned mandibular incisors of newborn wild-type (WT) and *Rac1*$^{-/-}$ mice. Amelogenin expression was detected along the developmental gradient of ameloblasts in newborn mandibular incisors from WT (A, C and E) or *Rac1*$^{-/-}$ (B, D and F) mice. Specific regions from *Rac1*$^{-/-}$ mice at an early secretory stage (box D) or a presecretory stage (box F) of development were compared with similar regions from WT animals (boxes C and E). Am, ameloblast; Od, odontoblast.

fibroblast F-actin and the organization of actin cytoskeleton (40). RAC1 and CDC42 are suggested to affect cell polarity, cell spreading, and filopodia formation of the dental epithelium mediated by laminin-10/11 (41). In our study, disruption of *Rac1* in dental epithelium has been shown to interfere with cytoskeleton organization of ameloblasts and cell–cell and cell–matrix contacts, as evidenced by the disorganized secretory ameloblasts, resulting in the loss of function for ameloblasts to regulate enamel matrix synthesis and mineralization.

In summary, RAC1 protein plays a crucial role in tooth enamel formation. The mechanism involved in RAC1 signaling in the dental epithelium needs to be further explored so that its role in modulating cell–matrix interaction during enamel formation can be better understood.

Acknowledgements – The University of Southern California Molecular Imaging Center provided MicroCAT II imaging and the authors are grateful for support from the National Institute for Dental and Craniofacial Research, NIH, USPHS through R01DE015920.

Conflicts of interest – The authors declare no conflicts of interest.

References

1. Thesleff I. The genetic basis of tooth development and dental defects. *Am J Med Genet A* 2006; **140**: 2530–2535.
2. Jernvall J, Jung HS. Genotype, phenotype, and developmental biology of molar tooth characters. *Am J Phys Anthropol* 2000; **113** (Suppl 31): 171–190.
3. Fincham AG, Moradian-Oldak J, Simmer JP. The structural biology of the developing dental enamel matrix. *J Struct Biol* 1999; **126**: 270–299.
4. Sugihara K, Nakatsuji N, Nakamura K, Nakao K, Hashimoto R, Otani H, Sakagami H, Kondo H, Nozawa S, Aiba A, Katsuki M. Rac1 is required for the formation of three germ layers during gastrulation. *Oncogene* 1998; **17**: 3427–3433.
5. Noritake J, Fukata M, Sato K, Nakagawa M, Watanabe T, Izumi N, Wang S, Fukata Y, Kaibuchi K. Positive role of IQGAP1, an effector of Rac1, in actin-meshwork formation at sites of cell-cell contact. *Mol Biol Cell* 2004; **15**: 1065–1076.
6. Thomas PS, Kim J, Nunez S, Glogauer M, Kaartinen V. Neural crest cell-specific deletion of Rac1 results in defective cell–matrix interactions and severe craniofacial and cardiovascular malformations. *Dev Biol* 2010; **340**: 613–625.
7. Vidali L, Chen F, Cicchetti G, Ohta Y, Kwiatkowski DJ. Rac1-null mouse embryonic fibroblasts are motile and respond to platelet-derived growth factor. *Mol Biol Cell* 2006; **17**: 2377–2390.
8. Liu S, Kapoor M, Leask A. Rac1 expression by fibroblasts is required for tissue repair in vivo. *Am J Pathol* 2009; **174**: 1847–1856.
9. Cerny R. [Mineralized dental enamel matrix proteins]. *Bratisl Lek Listy* 2000; **101**: 288–293.
10. Bei M, Stowell S, Maas R. Msx2 controls ameloblast terminal differentiation. *Dev Dyn* 2004; **231**: 758–765.
11. Huang Z, Sargeant TD, Hulvat JF, Mata A, Bringas P Jr, Koh CY, Stupp SI, Snead ML. Bioactive nanofibers instruct cells to proliferate and differentiate during enamel regeneration. *J Bone Miner Res* 2008; **23**: 19950–20060.
12. Filipenko NR, Attwell S, Roskelley C, Dedhar S. Integrin-linked kinase activity regulates Rac- and Cdc42-mediated actin cytoskeleton reorganization via alpha-PIX. *Oncogene* 2005; **24**: 5837–5849.
13. DeMali KA, Wennerberg K, Burridge K. Integrin signaling to the actin cytoskeleton. *Curr Opin Cell Biol* 2003; **15**: 572–582.
14. Boyde A. Correlation of ameloblast size with enamel prism pattern: use of scanning electron microscope to make surface area measurements. *Z Zellforsch Mikrosk Anat* 1969; **93**: 583–593.
15. Reith EJ, Boyde A. The arrangement of ameloblasts on the surface of maturing enamel of the rat incisor tooth. *J Anat* 1981; **133**: 381–388.
16. Nishikawa S, Fujiwara K, Kitamura H. Formation of the tooth enamel rod pattern and the cytoskeletal organization in secretory ameloblasts of the rat incisor. *Eur J Cell Biol* 1988; **47**: 222–232.
17. Cutroneo G, Anastasi G, Donadio N, Favaloro A, Micali A, Nastro Siniscalchi R, Santoro G, Trimarchi F. Actin-associated proteins in ameloblast differentiation. *Cells Tissues Organs* 2002; **171**: 128–134.
18. Glogauer M, Marchal CC, Zhu F, Worku A, Clausen BE, Foerster I, Marks P, Downey GP, Dinauer M, Kwiatkowski DJ. Rac1 deletion in mouse neutrophils has selective effects on neutrophil functions. *J Immunol* 2003; **170**: 5652–5657.
19. Xu Y, Zhou YL, Gonzalez FJ, Snead ML. CCAAT/enhancer-binding protein delta (C/EBPdelta) maintains amelogenin expression in the absence of C/EBPalpha in vivo. *J Biol Chem* 2007; **282**: 29882–29889.
20. Snead ML. Enamel biology logodaedaly: getting to the root of the problem, or "who's on first...". *J Bone Miner Res* 1996; **11**: 899–904.
21. Krebsbach PH, Lee SK, Matsuki Y, Kozak CA, Yamada KM, Yamada Y. Full-length sequence, localization, and chromosomal mapping of ameloblastin. A novel tooth-specific gene. *J Biol Chem* 1996; **271**: 4431–4435.
22. Couwenhoven RI, Luo W, Snead ML. Co-localization of EGF transcripts and peptides by combined immunohistochemistry and in situ hybridization. *J Histochem Cytochem* 1990; **38**: 1853–1857.
23. Chrostek A, Wu X, Quondamatteo F, Hu R, Sanecka A, Niemann C, Langbein L, Haase I, Brakebusch C. Rac1 is crucial for hair follicle integrity but is not essential for maintenance of the epidermis. *Mol Cell Biol* 2006; **26**: 6957–6970.
24. Castilho RM, Squarize CH, Patel V, Millar SE, Zheng Y, Molinolo A, Gutkind JS. Requirement of Rac1 distinguishes follicular from interfollicular epithelial stem cells. *Oncogene* 2007; **26**: 5078–5085.
25. Paine ML, Snead ML. Tooth developmental biology: disruptions to enamel-matrix assembly and its impact on biomineralization. *Orthod Craniofac Res* 2005; **8**: 239–251.
26. Snead ML. Amelogenin protein exhibits a modular design: implications for form and function. *Connect Tissue Res* 2003; **44** (Suppl 1): 47–51.
27. Rajpar MH, Harley K, Laing C, Davies RM, Dixon MJ. Mutation of the gene encoding the enamel-specific protein, enamelin, causes autosomal-dominant amelogenesis imperfecta. *Hum Mol Genet* 2001; **10**: 1673–1677.
28. Wright JT. The molecular etiologies and associated phenotypes of amelogenesis imperfecta. *Am J Med Genet A* 2006; **140**: 2547–2555.
29. Hart PS, Hart TC, Michalec MD, Ryu OH, Simmons D, Hong S, Wright JT. Mutation in kallikrein 4 causes autosomal recessive hypomaturation amelogenesis imperfecta. *J Med Genet* 2004; **41**: 545–549.
30. Hart PS, Aldred MJ, Crawford PJ, Wright NJ, Hart TC, Wright JT. Amelogenesis imperfecta phenotype-genotype correlations with two amelogenin gene mutations. *Arch Oral Biol* 2002; **47**: 261–265.
31. Biz MT, Marques MR, Crema VO, Moriscot AS, dos Santos MF. GTPases RhoA and Rac1 are important for amelogenin and DSPP expression during differentiation of ameloblasts and odontoblasts. *Cell Tissue Res* 2010; **340**: 459–470.

32. Li Y, Pugach MK, Kuehl MA, Peng L, Bouchard J, Hwang SY, Gibson CW. Dental enamel structure is altered by expression of dominant negative RhoA in ameloblasts. *Cells Tissues Organs* 2011; **194**: 227–231.
33. Fukumoto S, Kiba T, Hall B, Iehara N, Nakamura T, Longenecker G, Krebsbach PH, Nanci A, Kulkarni AB, Yamada Y. Ameloblastin is a cell adhesion molecule required for maintaining the differentiation state of ameloblasts. *J Cell Biol* 2004; **167**: 973–983.
34. Gibson CW, Collier PM, Yuan ZA, Chen E, Adeleke-Stainback P, Lim J, Rosenbloom J. Regulation of amelogenin gene expression. *Ciba Found Symp* 1997; **205**: 187–197; discussion 197–189.
35. Gibson CW, Yuan ZA, Hall B, Longenecker G, Chen E, Thyagarajan T, Sreenath T, Wright JT, Decker S, Piddington R, Harrison G, Kulkarni AB. Amelogenin-deficient mice display an amelogenesis imperfecta phenotype. *J Biol Chem* 2001; **276**: 31871–31875.
36. Hatakeyama J, Fukumoto S, Nakamura T, Haruyama N, Suzuki S, Hatakeyama Y, Shum L, Gibson CW, Yamada Y, Kulkarni AB. Synergistic roles of amelogenin and ameloblastin. *J Dent Res* 2009; **88**: 318–322.
37. Hunter GK, Curtis HA, Grynpas MD, Simmer JP, Fincham AG. Effects of recombinant amelogenin on hydroxyapatite formation in vitro. *Calcif Tissue Int* 1999; **65**: 226–231.
38. Fukumoto S, Yamada A, Nonaka K, Yamada Y. Essential roles of ameloblastin in maintaining ameloblast differentiation and enamel formation. *Cells Tissues Organs* 2005; **181**: 189–195.
39. Li Y, Decker S, Yuan ZA, Denbesten PK, Aragon MA, Jordan-Sciutto K, Abrams WR, Huh J, McDonald C, Chen E, MacDougall M, Gibson CW. Effects of sodium fluoride on the actin cytoskeleton of murine ameloblasts. *Arch Oral Biol* 2005; **50**: 681–688.
40. Albertinazzi C, Cattelino A, de Curtis I. Rac GTPases localize at sites of actin reorganization during dynamic remodeling of the cytoskeleton of normal embryonic fibroblasts. *J Cell Sci* 1999; **112** (Pt 21): 3821–3831.
41. Fukumoto S, Miner JH, Ida H, Fukumoto E, Yuasa K, Miyazaki H, Hoffman MP, Yamada Y. Laminin alpha5 is required for dental epithelium growth and polarity and the development of tooth bud and shape. *J Biol Chem* 2006; **281**: 5008–5016.